Infrared pattern based method for inspecting multi-nozzle spraying tools

OPEN ACCESS
IOP Publishing
Measurement Science and Technology
Meas. Sci. Technol. **34** (2023) 015902 (14pp)
https://doi.org/10.1088/1361-6501/ac963a

Infrared pattern based method for inspecting multi-nozzle spraying tools

Florian Schulz*, **Franziska Reincke and Frank Beyrau**

Lehrstuhl für Technische Thermodynamik, Otto-von-Guericke-Universität Magdeburg, Magdeburg, Germany

E-mail: florian.schulz@ovgu.de

Received 4 April 2022, revised 23 September 2022
Accepted for publication 29 September 2022
Published 19 October 2022

Abstract

Multi-nozzle spraying tools are applied in numerous industrial applications, one of the most common being die-casting. To ensure the quality of a cast product and to avoid production downtimes proper functioning is required, e.g. in terms of spray targeting, mass flow, or reproducibility. To enable regular functional controls of a spraying tool, we have developed a specific measuring principle based on monitoring the spray impact on a heated plate using infrared thermography. In this paper, the performance of the developed measuring principle is examined. The study is performed with a typical spraying tool from foundries, it has nine external mixing air–water nozzles, which are freely adjustable in their orientation. During an injection, the spray impacts a heated plate positioned in front of the spraying tool and creates a wetting pattern that is individual to each spraying tool, like a fingerprint. The recorded cooling pattern can be used to determine the position of the individual spray impact areas, the size of the spray impact areas, and the intensity of the cooling. Based on these parameters, conclusions can be drawn about the functionality of the water-bearing lines and the air-bearing lines—as well as the correct alignment of the individual nozzles. The result shows that the presented measuring principle leads to very high precision and reproducibility of the evaluated parameters. Thus, the developed measuring system enables detailed functional tests of complex spraying tools.

Keywords: nozzle testing, spray characterization, wetting pattern, infrared thermography

(Some figures may appear in colour only in the online journal)

1. Introduction

Spraying tools are used in various branches of industry, one of which is foundry technology. Here they are used, for example, to clean and wet casting molds with release agents or to cool castings. Before its use, a spraying tool has to be adapted individually to its task and the geometry of the object to be sprayed. Under the harsh conditions of a foundry, the nozzles are regularly soiled and even the geometric orientation of individual nozzles can unintentionally misalign. Even small changes from the original state can be enough to prevent the spraying tool from fulfilling its task properly; for example, a casting mound is no longer completely wetted with a release agent. As a consequence, reject products are manufactured, which in turn results in downtimes for maintenance. In order to avoid such cost-intensive production losses, the correct functioning of the spraying tools must be guaranteed at all times.

Since there is no appropriate measuring system for this purpose so far, a malfunction is often only discovered when problems occur. Then the spraying tool is typically checked visually, cleaned, and realigned by technicians. Unfortunately, the inner channels and bores cannot be checked and there is no convenient method to monitor the quality of the spray, as the multi-nozzle sprays are too complex to be visually investigated by the eye. Figure 1 gives an example of a modern multi-nozzle

* Author to whom any correspondence should be addressed.

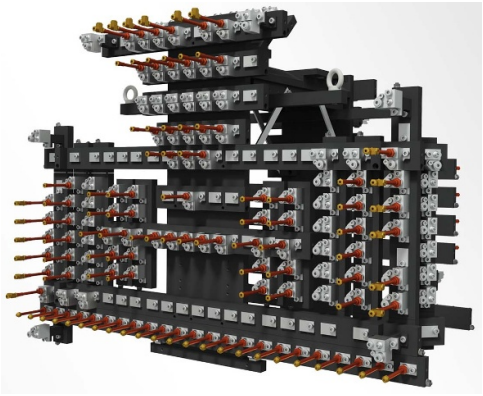

Figure 1. Example of a complex multi-nozzle spraying tool. Reproduced with permission from Wollin GmbH. www.wollin.de/de/Produkte/formspr%C3%BChen/powerspray-formsprueh werkzeug.html.

spraying tool with more than 100 nozzles. This example illustrates the difficulty of controlling the quality of a large number of spray jets that occur simultaneously. Ideally, the spray of a spraying tool would be inspected regularly, before each use. So that production downtimes are avoided and the spraying tool can be correctly adjusted if necessary.

Apart from visual inspection, there are only a few measurement techniques available to determine the required spray properties. A classical method to determine the temporally resolved penetration and the width of a spray jet is to record shadowgraphy images (Emberson *et al* 2016, Schulz and Beyrau 2017) or Mie-scattering images with high-speed cameras (Montanaro *et al* 2015, Kim *et al* 2018). However, the technique is limited to optically well-accessible spray jets. Considering multi-nozzle spraying tools only the spray jets at the edges are optically accessible, so the technique cannot be used to draw conclusions about jet core or individual nozzles in the center of multi-nozzle arrangements (Fansler and Parrish 2015).

A method to improve the optical accessibility of internal spray structures is the illumination with laser-light sheets (Zhang *et al* 2012, Hult and Mayer 2013). If such a light sheet is arranged perpendicular to the spray jet axis, the positions of the passing jets can be made visible, and, to a certain extent, conclusions can be drawn about the local spray densities (Serras-Pereira *et al* 2015). It is also possible to use a laser to excite a fluorescence signal. This can then be used to determine the liquid and gas distribution (Parrish and Zink 2013, Schulz *et al* 2016). Requirements regarding laser safety, the sensitivity to harsh conditions, the inaccessibility of dense sprays, and the high costs are disadvantages of using the light sheet techniques.

Droplet sizes and velocities can be determined locally in a small measuring volume with the aid of phase Doppler anemometry (Wigley *et al* 1999, Dafsari *et al* 2019). Beyond, the local distribution of the liquid mass in the spray can also be determined if the spray is systematically scanned. However, this procedure is very time-consuming and in very dense sprays, the measurement technique reaches its limits (Mantel 2017, Rahim and Dorairaju 2018). With respect to practical use in industrial applications for *in-situ* spray monitoring, the same disadvantages as with the laser-light sheets technique occur.

A more practical device to measure the spatially resolved mass flux of a spray is a patternator. However, there are different requirements the system has to meet. The size of the patternator must be equal to or bigger than the size of the spraying tool. One challenge for an adapted system is the required high spatial resolution, which is associated with a large number of collection openings and the necessary digital read-out. Moreover, there must be a way to efficiently clean a large number of small channels (Nocivelli *et al* 2017).

Considering practical industrial applications, it is often not essential to measure defined microscopic spray properties quantitatively. Rather, it is sufficient to record whether the spray properties still correspond to a target or reference state.

There is a new measurement method that records the wetting pattern generated by the spraying tool (Schulz *et al* 2021). For this purpose, a frosted pane is positioned in front of the spraying tool and the resulting wetting pattern is recorded by a camera on the back of the frosted pane. A change in the wetting pattern indicates a change in the spraying tool and, in the best case, allows conclusions to be drawn about the cause of the defect. This technique enables versatile defect detection, but also has weaknesses. For example, overlapping wetting areas cannot be kept apart and no conclusions can be drawn about the intensity of the spray/wall interaction. At the same time, the frosted pane must be cleaned after each injection and very good illumination must be ensured.

For a robust, cost-effective, and precise monitoring of spraying tools, we have developed a new infrared-based method. Here, the spray impinging on a heated target surface generates a specific cooling pattern that is recorded by an infrared camera. Spray monitoring is performed by recording a master cooling pattern from a new, well-aligned spraying tool. In between regular operation, a recorded control pattern is then compared with the recorded master pattern. Changes in the spray are detected utilizing deviations between the documented cooling patterns. The results allow conclusions about the causes or failures, such as misalignment or clogging of nozzles.

With the new measuring technique presented here, large multi-nozzle spraying tools can be inspected quickly and cost-effectively and the functionality can be documented over its life cycle. At the same time, the measuring system is robust against harsh conditions in foundries and is easy to operate. This enables production downtimes to be avoided and costs to be reduced.

2. Material and methods

2.1. Measurement technique

The central part of the setup is a heated metal sheet. Figure 2 shows the arrangement of the heated sheet in front of the spraying tool. For the detection of the cooling pattern—which forms on the backside of the heated sheet—an ImageIR 8300 infrared camera from InfraTec with 640 × 512 pixels with an

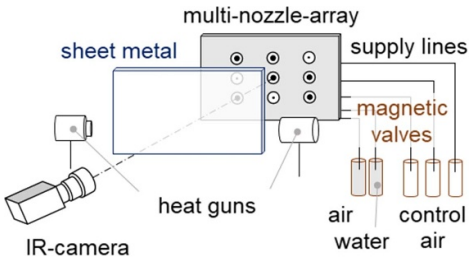

Figure 2. Schematic of the experimental setup for the infrared-based detection of cooling patterns on a heated metal sheet.

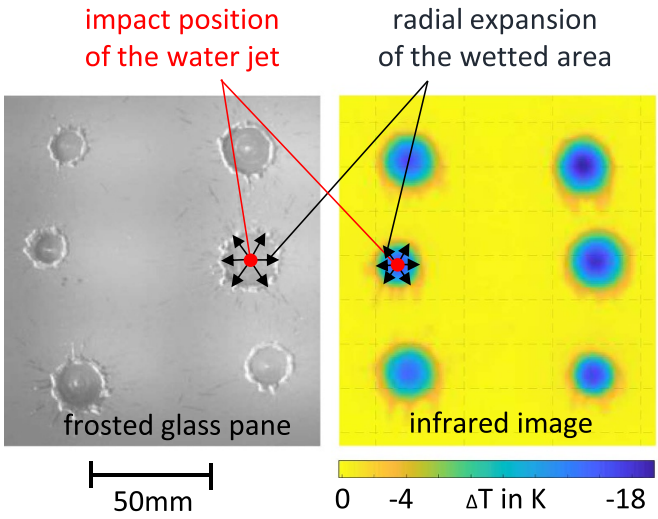

Figure 3. Left: image from the backside of a frosted glass pane during impingement of six straight water jets; right: processed temperature field after the impingement of straight water jets from the backside of a heated metal sheet.

$f = 50$ mm lens was used. It operates in the short and medium wave range and covers a spectrum of 1.5–5.7 µm. The thermal resolution of the camera is 20 mK in the calibrated range of 20 °C–100 °C in applied full-frame mode. For the entire measurement campaign, a recording frequency of 100 Hz and an exposure time of 500 µs are used. An example of an infrared cooling pattern after spray impingement is shown in the right part of figure 3. For comparison, the image of a wetting pattern formed on a frosted pane is shown here on the left. In the example shown, the impinging water jets only have a diameter of less than 1 mm, but the momentum drives the water radially outward. This forms circular wetting areas, which become larger with increasing time.

When using sprays at ambient temperature, the sheet must be heated above ambient temperature to generate cooling patterns on the surface. Here, due to the high flexibility, the sheet was heated by two hot air guns. But other methods of heating such as direct electric heating and radiant sources can also be applied. In the applied setup a homogeneous average sheet temperature of 52 °C was set before the start of injection and used throughout the measuring campaign.

To achieve the desired average plate temperature, the metal plate is first heated above the setpoint. Then the hot air guns are switched off. Now the average plate temperature slowly decreases and at the same time, the temperature on the plate surface is homogenized by transverse heat conduction. The infrared (IR) camera enables continuous recording of the mean surface temperature and triggering when the preset temperature value was reached. So, the injection process is started when the desired average value of 52 °C is reached over the metal surface.

At this step, the maximum local deviations from the mean plate temperature are less than 1.5 K. Due to the reproducibility of the spray measurement results, it can be assumed that the small fluctuations that occur in the temperature distribution of the plate surface do not have a decisive influence on the significance of the measurement results.

With the prevailing temperatures and the associated low radiation intensities, a high emissivity of the surface is desirable to obtain meaningful images. Therefore, the metal sheet was coated with a black graphite coating on the backside. The coating has an emissivity of 0.9 and a thickness of 30 µm. Preliminary investigations have shown that for high sensitivity of the measuring principle a low sheet thickness is preferable (Schulz *et al* 2014). At the same time, it is easier to achieve homogeneous tempering with increasing sheet thickness. The plate material used was stainless steel (1.4016/ASTM 430). The finally used sheet thickness of 0.5 mm represents a compromise between sensitivity, homogeneity, and mechanical stability for the test setup.

2.2. *Spraying tool*

For this investigation, a nozzle array originating from foundry technology was used. The nozzle array consists of three horizontally arranged supply modules, each of which is equipped with three nozzles. With the nine nozzles installed, the behavior of a characteristic spraying tool can be represented.

The spraying tool includes central solenoid valves for opening and closing the air and water supply, controlled by 5 V transistor-transistor-logic (TTL) signals. Before the start of an injection process, the water pressure and the air pressure are only present up to the solenoid valves. As the valves are opened, the pressure in the corresponding supply module rises to the nozzles.

The supply modules share the water connection and the connection for the atomizing air. However, each supply module has a separate connection for control air. With the help of the control air, the pneumatic valves inside the nozzles are opened to allow water to flow through. The operating principle of the nozzles is shown in figure 4. The nozzles are external mixing air–water nozzles, where compressed air atomizes the emerging water jet.

To allow high flexibility, the spraying tool enables the use of nozzles of different sizes. To account for the influence of the nozzle size, the applied tool is equipped with three small nozzles and six large nozzles. Figure 4 shows images of the two nozzle types, illustrating the different sizes of the hole diameters. The positioning of the different nozzles is illustrated in figure 2 by the size of the dots in the circles.

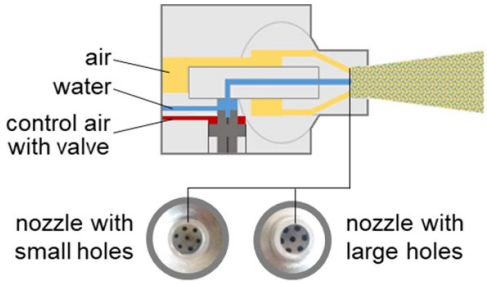

Figure 4. Air–water nozzles with internal pneumatic valve and nozzle images with hole diameters of 0.6 mm and 1 mm.

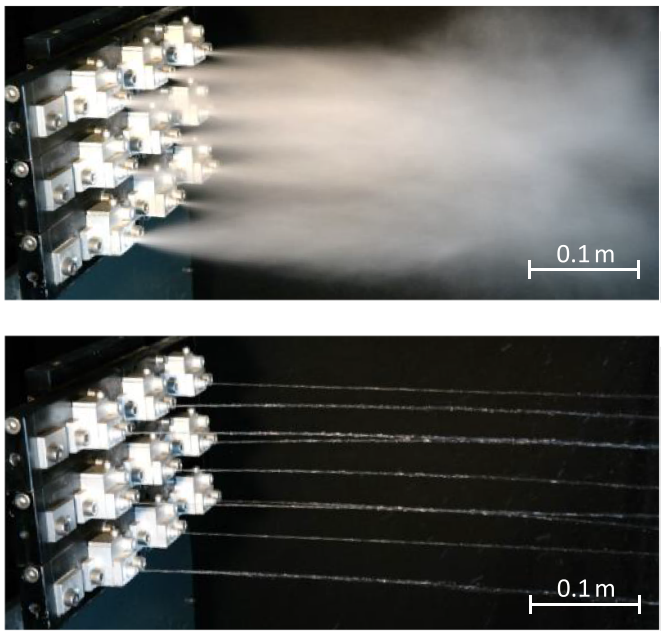

Figure 5. Multi-nozzle spraying tool with nine nozzles; top: injection of a spray with the atomizing-air switched on; bottom: injection of straight water jets with the atomizing-air switched off.

There is an interesting working characteristic of the spraying tool, which can be used to determine its correct functioning. With the atomizing air switched off, it is possible to only inject a thin water jet. This operating mode will be referred to as straight water injection. An injection of a full spray appears when the atomizing air is switched on. Figure 5 shows the first operating mode with straight water injection and figure 1 shows the second operating mode with spray injection. A third operating mode allows the sole injection of air.

The three working modes enable separate testing of different tool components and different properties. Here, the functionality of the water-bearing system can be tested with the straight water injection. Similarly, the functionality of the air-bearing system can be tested with the sole injection of atomizing air. Finally, the overall performance becomes clear with the spray injection.

In the experiments, it is important to keep the boundary conditions as constant as possible. For this purpose, the air pressure is adjusted to 5 bar with the help of a compressor with air reserve. For the water, an expansion vessel is used, in which the gas side is filled with nitrogen. Thereby, the water pressure is kept constant at 4 bar. The temperature of the water and air are at equilibrium with the constant ambient temperature of 22 °C. The distance between the nozzles and the metal plate is set at 11 cm, which was found to be favorable in a preliminary investigation. The distance represents an optimum between a short spray path and the geometric conditions of real spraying tools, which cannot be positioned at an arbitrary distance from the metal sheet. It is close enough to avoid overlapping of the spray impact areas but far enough to detect even small changes in nozzle orientation. The injection durations are controlled by the length of the TTL signals. Depending on the operating mode the belonging solenoid valves are triggered for 150 ms.

2.3. Image processing

The image processing aims to get further information from the cooling patterns. For example, it is intended to characterize individual nozzles of the nozzle array. Important parameters to be evaluated are the positions of the impact areas, the sizes of the individual impact areas, and the intensities of the spray/wall interaction. For this purpose, an image post-processing algorithm is developed using Matlab. The algorithm includes the import of image data, background subtraction, binarization, determination of the wetted areas, determination of centers, and determination of cooling effect.

For the purpose of comparability of different measuring series, it is necessary to set the initial temperature of the metal plate always to the same value. Homogeneous tempering of the metal plate to 52 °C was achieved by two hot air guns, as described in the experimental setup. The recording of the initial temperature profile on the metal plate is referred to as the background image in the following. An example of the temperature distribution on the metal plate before the injection is shown in figure 6.

For the evaluation, the temperature changes ($\Delta T_{x,y,t}$) generated by the injections are extracted from the raw infrared images of the spray patterns. These describe the decrease in the temperature of the metal plate. For every time step (t), these are calculated by subtracting the background image ($T_{x,y,\text{initial}}$), which is present right before the start of the injection, from the current temperature field ($T_{x,y,t}$):

$$\Delta T_{x,y,t} = T_{x,y,t} - T_{x,y,\text{initial}} \tag{1}$$

while x and y are the pixel positions of the lines and rows of the temperature field. The image of the temperature differences resulting from the subtraction is shown in figure 6.

For the determination of the size of the wetting areas and wetting area positions, the binarization is performed in a final step based on a previously determined threshold value of 5 K. The influence of the threshold value on the results is described in the following section.

2.3.1. Size of the wetted regions. Based on the fields of temperature differences the wetting regions caused by jet impingement are found by applying a threshold value. The threshold

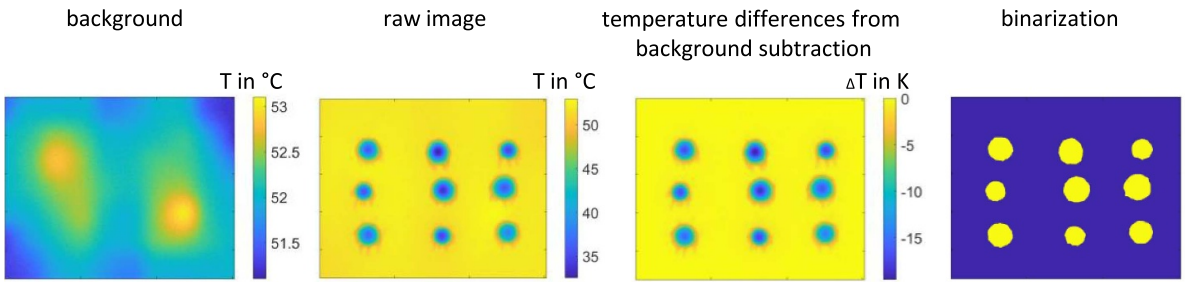

Figure 6. Image processing steps from raw images to binarized images, for an example of pure water injection.

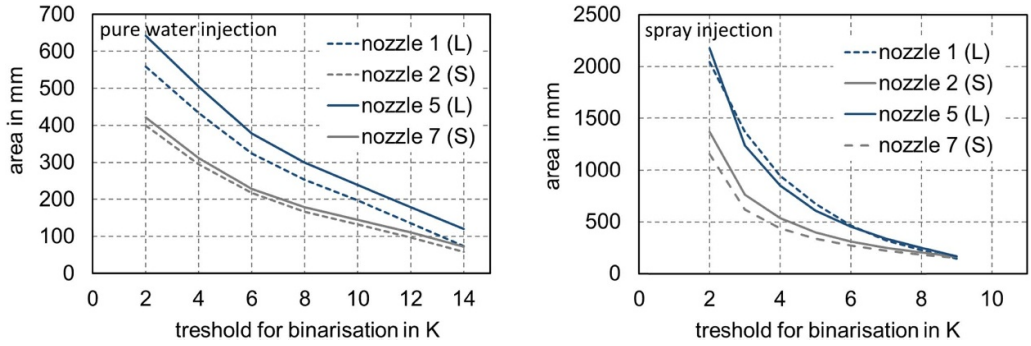

Figure 7. The calculated size of the wetting areas as function of the threshold value, each for two large nozzles (L) and two small nozzles (S); left: pure water injection; right: spray injection.

value here stands for the absolute value of the temperature reduction from the fields of temperature differences. From the resulting regions, the size—as a characteristic parameter—can easily be obtained by counting the number of pixels and applying the resolution of 0.137 mm^2 $pixel^{-1}$.

To show the influence of the threshold value on the calculated size of the wetting area, the calculated areas are plotted against the threshold value in figure 7. As an example, the measurement data of figures 9 and 10 are used. For pure water injection (left diagram), threshold values from 2 K to 14 K were investigated. Since the maximum cooling is lower with spray injection, only maximum threshold values up to 9 K were investigated here. For better traceability and clarity, the diagrams contain results only for four nozzles, two with small holes (nozzle number 2 and 7) and two with large holes (nozzle number 1 and 5).

In general, it can be stated that the threshold values can range between a possible minimum value and a maximum value. The minimum value is given by the undetermined temperature change on the sheet surface, which is in the range of less than 1 K. Undetermined temperature changes can result from unwanted convection flows and noise. On the other hand the maximum value is limited by the maximum temperature drop.

The diagrams show, that the detected wetting area decreases with increasing threshold values. Nozzles with small nozzle holes tend to produce smaller wetting areas. At the same time, the detected wetting areas related to the same threshold values are larger for spray injection (right) than for pure water injection (left). In the present measurement method, the dependence of the calculated wetting area on the threshold value is actually of secondary importance. Much more decisive here is the reproducibility of the measurement results for any threshold value. This is given, as can be shown in the results section. For the later documentation of results, the evaluation is limited to the use of a uniform threshold value of 5 K. This is small enough to detect even small humidifications but at the same time large enough to exclude the detection of unwanted cooling effects, such as unknown convection flows.

2.3.2. Centers of the wetted regions. Two methods are tested to determine the centers of the wetted areas. In method A, the centers of geometric gravity of the binarized regions are determined in a way, that the same number of pixels is above and below as well as left and right from the center point. With method B, the position of the strongest cooling is identified. For this, the fields of temperature differences themselves are taken to find the position of the lowest temperature within the previously defined wetted area.

While method B is independent of the threshold value, method A can theoretically be dependent on the threshold value. To test this dependence, the calculated center point values are plotted against the threshold in figure 9. Again, the IR images of figures 8 and 9 are used as examples. The plots in figure 10 show the center point values of the individual wetting surfaces determined from the binarized images using the

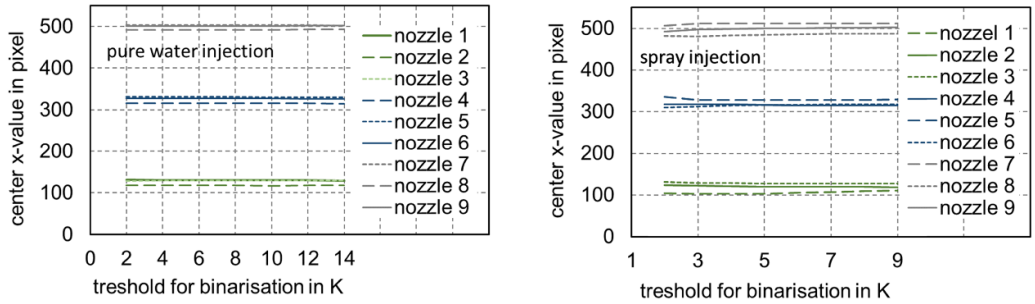

Figure 8. The course of the x-values of the center positions of the wetted surfaces as function of the threshold; left: pure water injection; right: spray injection.

geometric gravity method. For the sake of clarity, only the x-values are shown here. The threshold values correspond to the values of the previous figure 7.

It is clear that the center values for both water-only injection (left) and spray injection (right) are almost independent of the choice of the threshold value. This is especially true for the intermediate threshold range. Only for very small and very large threshold values do small deviations occur. A certain threshold value independence of the results is generally advantageous. This is because changes in the absolute temperature reduction in a wetting area would have less effect on the position determination. For the present measurement task, however, this is only of secondary importance because the reproducible determination of the position of a wetting surface is the primary objective.

In the more constant threshold value range from 4 K to 12 K, the maximum threshold value-related change in the center point value occurs at nozzle 5 for pure water injection. Here the x-value changes by 0.49 mm and the y-value by 0.25 mm. With spray injection, the maximum threshold-related change in the center point value occurs at nozzle 8. The x-value increases with an increasing threshold value by 1.45 mm and the y-value by 0.49 mm. Regarding the selection of the threshold value, it can be stated that the threshold value should not be selected too high, since even small temperature decreases indicate wetting. The selected threshold value of 5 K is low and at the same time in the range in which position results are relatively independent of the threshold value.

3. Results and discussion

To characterize the performance of the measurement method presented, various tests are carried out below, using the test spraying tool described. One after the other, the evaluation parameters, (a) center positions, (b) sizes and (c) temperature reduction of the wetted areas are determined. The focus is on the reproducibility and precision of the measurement results. The three evaluation parameters are measured for each operating mode: pure water injection, spray injection, and air injection. The chapter concludes with a summary of how the measurement results can be used to detect defects in a spraying tool.

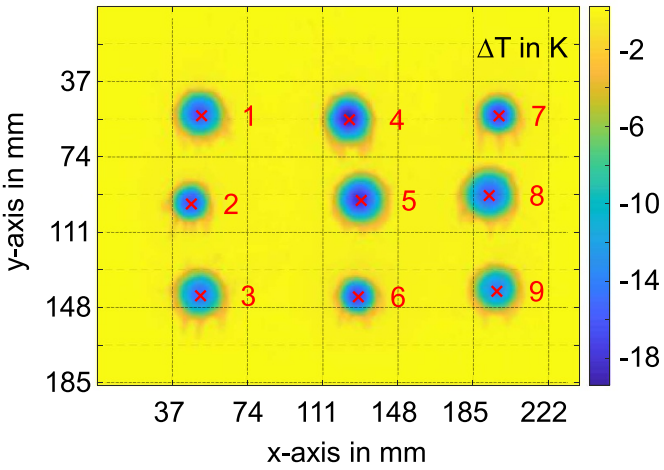

Figure 9. Cooling pattern resulting from straight water injection with crosses marking the individual center point positions of the wetted areas.

3.1. Determination of the center points of the wetted areas

The position of the center points of the jet impingement areas turned out to be a suitable parameter to check the alignment of the nozzles. In the following, it is examined to what extent the center points can be determined reproducibly. The measurements presented are carried out first with straight water injection and thereafter with spray injection.

Two different methods, which are explained in the image processing section, are tested for the determination of the center points. In method A, the centers of gravity of the individual wetting areas are calculated. In method B, the positions of the maximum temperature drop are determined and used as center points.

3.2. Center points of straight water injection

For these measurements, the previously defined basic settings are used and ten repetitions are carried out for each measurement. The coordinate system shown in figure 9 is used to define the positions of the center points. The results for the injection of straight water jets are summarized in table 1. Thereby x-pos and y-pos are the mean values of the measured x and y

Table 1. Positions of center points for straight water injection using evaluation methods A (center of gravity) and B (position of lowest temperature) including standard deviations, whereby for method B the deviations Δx_{AB} and Δy_{AB} to the positions determined with method A are listed.

			x-pos (mm)	σ_{xA} (mm)	y-pos (mm)	σ_{yA} (mm)	Δx_{AB} (mm)	σ_{xB} (mm)	Δy_{AB} (mm)	σ_{yB} (mm)
Column	Row	Nozzle holes	Method A				Method B			
1	1	Large	51.8	0.25	54.6	0.24	0.7	0.15	**2.4**	0.53
	2	Small	46.7	0.33	97.8	0.35	1.1	1.15	1.2	0.84
	3	Large	51.2	0.24	142.8	0.25	−0.6	**2.26**	1.6	0.99
2	1	Large	124.3	0.22	57.7	0.37	0.3	0.5	1.6	1.07
	2	Large	130.4	**0.39**	96.7	**0.42**	**1.3**	1.2	1.4	**1.71**
	3	Small	128.8	0.22	143.6	0.31	0.6	1.45	1.1	0.44
3	1	Small	197.6	0.27	54.7	0.25	0.1	0.66	1.3	0.62
	2	Large	192.7	0.23	94	0.27	0.6	1.81	2.2	1.35
	3	Large	196.3	0.24	140	0.28	1.0	2.07	2.0	1.23

positions of the individual center points of the impingement area of each nozzle, resulting from method A. It can be seen that the determination of the centers using method A achieves very reproducible results with maximum standard deviations (σ_x, σ_y) of 0.39 mm in the x-direction and 0.42 mm in the y-direction. It should also be noted at this point that this standard deviation primarily reflects how strongly the orientation of the water jet varies from injection to injection.

In table 1 the deviations between method A and method B are displayed by the values of Δx_{AB} and Δy_{AB}. It is noticeable that the positions of the maximum temperature reductions found with method B deviate only slightly from the center point positions found with method A. In x-direction, there are average deviations of up to 1.3 mm and in y-direction up to 2.4 mm. Compared to method A the standard deviations of the center points for method B are considerably larger with maximum values of 2.26 mm and 1.71 mm in x- and y-direction. This precision still results in quite high sensitivity. Therefore, both methods can be used to test the alignment of the nozzles, whereby the advantage of method A is the higher precision and the advantage of method B is the lower calculation effort. The selection of the method may also depend on the type of spray.

With the help of the measured data of the straight water injection, it is possible to carry out the functional control of the water-carrying pipes and the nozzle alignment. If now the atomizing air is added, changes in the air-bearing system can be detected, as well. If, for example, single air-carrying holes of a nozzle (holes at the outer circumference in figure 4) are blocked or dirty, this would lead to a shift of the resulting center point. The ability to detect such phenomena is a great advantage in practical applications.

3.3. Center points of spray injection

The second operation mode investigated is the injection of a spray. An example of the cooling pattern is shown in figure 10. Based on such images, the positions of the wetting areas are determined. Table 2 shows the calculated center points for the injection of a spray. The centers of the atomized jets are determined by method A with a standard deviation of less than 1.12 mm in x-direction and less than 0.87 mm in y-direction. At the same time, the calculated center points of both methods

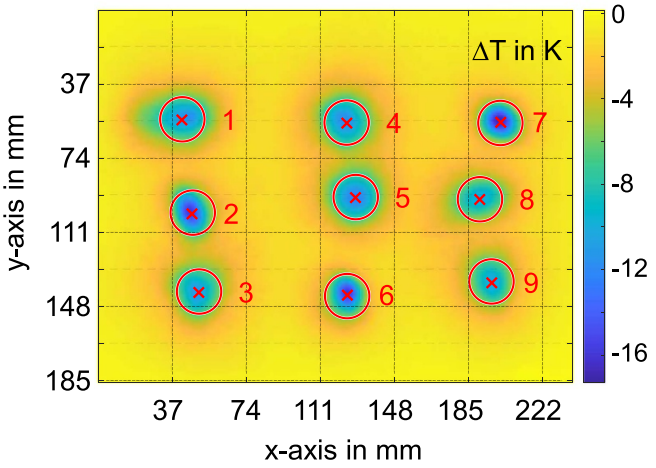

Figure 10. Cooling pattern resulting from spray injection with crosses marking the center points of the individual positions of the wetted areas.

are close to each other, which in turn is indicated by the differences (Δx_{AB} and Δy_{AB}) between the determined center points of the two methods. The differences of the calculated center positions have a maximum value of 1.7 mm on the x-axis and 2.8 mm on the y-axis.

When the center points are determined by method B, standard deviations up to 1.45 mm in x-direction and 1.69 mm in y-direction are obtained. Accordingly, the standard deviations in case of a spray injection are higher compared to the straight water injection. However, this is reasonable since the width of the jet is increased when the liquid is atomized. Thereby the impingement areas will increase and the cooling on the metal sheet is less focused. The values obtained represent a very high precision of repeat tests. This means that even single tests provide very accurate measurement results. If higher accuracies are required, it is possible to perform multiple tests to determine reliable average values.

Furthermore, for the characterization of the nozzles it is interesting to know: how much the jet impingement position shifts, when the atomization air is switched on. The offset values between the straight water center points and the spray center points give information about the relationship between

Table 2. Positions of center points for spray injection using evaluation methods A and B including standard deviations, whereby for method B the deviations Δx_{AB} and Δy_{AB} to the positions determined with method A are listed.

			x-pos (mm)	σ_{xA} (mm)	y-pos (mm)	σ_{yA} (mm)	Δx_{AB} (mm)	σ_{xB} (mm)	Δy_{AB} (mm)	σ_{yB} (mm)
Column	Row	Nozzle holes	Method A				Method B			
1	1	Large	46.4	0.32	99.8	**0.87**	0.2	0.35	**−2.8**	**1.69**
	2	Small	50.6	0.26	140.7	0.28	0.1	0.52	1.2	0.86
	3	Large	124.2	0.21	55.2	0.23	−0.4	0.58	0.7	0.95
2	1	Large	127.3	1.12	94.9	0.85	0.9	0.97	−0.9	1.39
	2	Large	124.2	0.28	145.5	0.77	0.6	0.5	−1.3	0.92
	3	Small	199.8	0.40	56.3	0.29	0.5	0.6	0.0	0.39
3	1	Small	190.3	0.32	95.1	0.19	**1.7**	**1.45**	0.2	1.15
	2	Large	196.4	0.23	135.5	0.16	0.5	0.78	1.1	0.84
	3	Large	46.4	0.32	99.8	0.87	0.2	0.35	−2.8	1.69

Table 3. Offset values between the center point positions comparing the injection of straight water jets and the injection of a spray using method A.

Column	Row	Nozzle holes	Δx (mm)	Δy (mm)
1	1	Large	−0.3	**2.1**
	2	Small	−0.6	−2.1
	3	Large	−0.1	−2.4
2	1	Large	−3.1	−1.8
	2	Large	**−4.6**	1.9
	3	Small	**2.2**	1.6
3	1	Small	−2.4	1.1
	2	Large	0.1	**−4.4**
	3	Large	−0.3	2.1

airflow and water jet. These offset values are derived by subtracting the center points of straight water injection and the center points of spray injection. The results are shown in table 3, while the values of method A are used for the comparisons, and the straight water injection is considered as a reference.

The offset values between the centers of the two types of injection range from −4.6 mm to 2.2 mm in x-direction and from −4.4 mm to 2.1 mm in y-direction. Since these shifts are significantly higher than the standard deviations measured before, it can be concluded that the application of the atomization air leads to a shift of the jet impingement positions. This is due to the inhomogeneity of the air supply and the turbulence created in the spray, among other things. The results also show that the position of the jet impingement points does not only depend on the geometric alignment of the nozzles, but also on the design and condition of the nozzle bores.

3.4. Determination of the sizes of the wetted areas

There may be malfunctions that do not result in a change of position of the center points. These include certain blockages that only lead to a reduction in mass flux. One parameter that might allow conclusions about the mass flux is the size of the wetted area.

To be able to estimate the mass fluxes occurring, the mass fluxes were measured under various boundary conditions before the start of the infrared measurements. For this purpose, the water emerging from the nozzles during injection was collected directly at the nozzle outlet. The injected water mass was determined by weighing on a precision balance. This was carried out for different water (injection) pressures and separately for the small and large nozzles. More detailed results can be found in (Schulz *et al* 2021). As expected, mass fluxes increase with increasing water pressure. Under the injection conditions of the IR investigations at a water pressure of 4 bar, average mass fluxes of 4.3 g s^{-1} for the small nozzles and 5.6 g s^{-1} for the large nozzles were obtained. Based on these investigations, it can be assumed that disturbances affecting the flow diameter or the water pressure at the nozzle outlet cause a change in the mass flux.

In addition to the mass flux measurements, we have carried out preliminary studies using the frosted glass pane (figure 3), in which we investigated the influence of the water (injection) pressure on the wetting area. Here, increased water pressure led to larger wetting areas. Therefore, we expect measurable differences in the sizes of the wetted areas. It remains to be clarified whether the results of the individual nozzles are reproducible enough to detect possible changes.

The following determination of the sizes of the wetted areas is based on a threshold value for the cooling, as explained in the image processing section. For the evaluation of the sizes, the measurements are carried out first with the straight water injection and thereafter with the spray injection.

3.4.1. Wetted area of straight water injection. In a first step, it is now to be checked whether there is a detectable difference between nozzles with large boreholes and nozzles with small boreholes. The determination of the wetted areas is performed with straight water injection at standard settings. Since the wetting area increases with increasing time, figure 11 displays the area-time diagram.

For the preparation of the graphs, the wetted areas of the present nozzles with large holes (six nozzles) and the nozzle with small holes (three nozzles) are averaged, whereby the

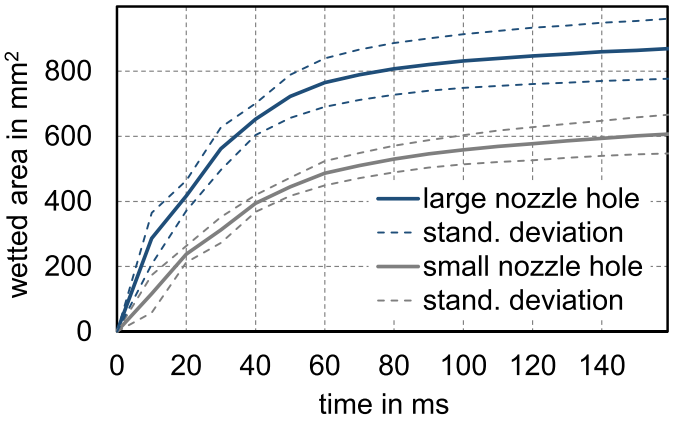

Figure 11. Progression of the wetted areas over time resulting from straight water injection, mean values of ten repetitions.

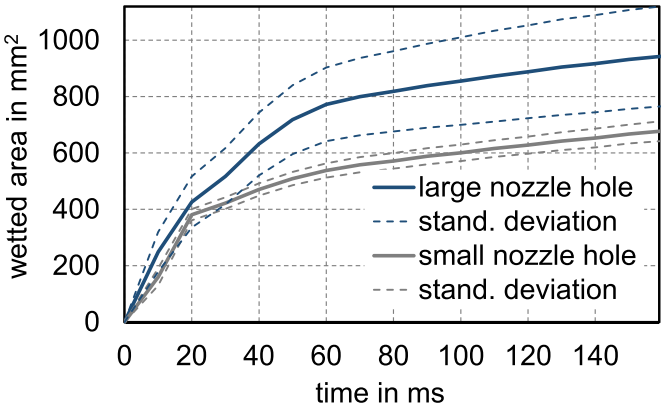

Figure 12. Progression of the wetted areas over time resulting from spray injection; mean values of ten repetitions.

measurement was repeated ten times. In the beginning, there is a strong increase in the area, from about 60 ms the curve flattens. To compare different nozzles or the condition of a spraying tool, entire curves can be compared or a single time step must be selected.

The dotted lines around the mean values represent the standard deviation. The diagram shows that the nozzles within a group show clear differences in the size of the produced wetting area. Since both nozzle groups are clearly different from each other, a proper distinction between large and small nozzles is possible. Consequently, the method of measuring the wetting area is sensitive to changes in the nozzle hole diameter and it can be used to monitor the stability of the injection behavior of individual nozzles over their life cycle.

If the measuring principle were applied in an industrial case, a reduction in the wetting area of a nozzle would indicate a clogging of this individual nozzle. If, on the other hand, the wetting area of all nozzles is reduced, this could indicate a drop in water pressure or clogging of the central water supply.

3.4.2. Wetted area of spray injection. For the straight water injection, the wetting area results from the radial expansion of the impinging water on the metal plate, as shown in figure 3. If we now additionally switch on the atomizing air, the process of wetting changes. The spray jets take up an increased volume and the cross-sectional area of the jets is significantly larger compared to a straight water jet. Therefore—in the case of spray injection—the sizes of the wetting area during spray injection correspond approximately to the cross-sectional area of the spray plumes. In the case of spray injection, the sizes of the wetted area allow statements about the intensity of atomization.

To visualize the effect of the nozzle hole size on the wetted area resulting from spray injection, the wetted areas are plotted in figure 12. The diagram reveals that the absolute sizes of the wetted areas are slightly larger compared to straight water injection, while the general slope is rather similar.

We can find a clear difference between large and small nozzles and we can identify the size of the footprint of a single spray plume. The fact that the nozzles with large bores wet a larger area was expected because the larger air volume flux causes a larger expansion of the spray jet. With the aid of the present investigation of the wetting areas, it has now been demonstrated that the spray jet characteristic influenced by the air volume flow can be determined by the size of the wetting areas. This finding allows far-reaching conclusions to be drawn. It can be stated that, if the wetted area of a single footprint changes from the master record to the control record, changes or problems with the belonging nozzle are found, e.g. clogging of the air carrying holes. If instead, the wetted areas of all nozzles changed simultaneously, there is likely a problem with the air carrying system (e.g. the air pressure).

3.5. Determination of the cooling effect

A further important parameter that might allow conclusions about the state of the spraying tool is the cooling performance. The determination of the cooling characteristic is possible since the temperature of the metal sheet is continuously recorded by IR camera. The local rate of heat flow between spray and metal sheet is proportional to the measurable temperature reduction of the metal sheet.

For a simplified determination, certain assumptions have to be made, which in turn lead to a degree of deviation from the true heat fluxes. Assuming that the Biot number approaches zero, a constant temperature can be assumed across the sheet thickness. Considering the present conditions, the Biot number would be below 0.1 for heat transfer coefficients up to 5000 W m^{-2} K^{-1}. At the same time, the measurement durations are very short, around 100 ms. This allows the transverse heat conduction within the sheet to be neglected during a recording. Under these conditions, the occurring heat flows can be estimated with the following equation:

$$\dot{Q}_{xy}(t) = M_{\mathrm{metal}} \cdot c_{\mathrm{metal}} \cdot \frac{\mathrm{d}T_{\mathrm{metal},xy}(t)}{\mathrm{d}t} \tag{2}$$

with $\dot{Q}_{xy}$, representing the local rate of heat flow and $\mathrm{d}T_{\mathrm{metal},xy}(t)$, representing the temperature change measured by

the camera. Both values are related to the area, xy, represented by a camera pixel. The values must always be related to a specific time t. The mass, M_{metal}, refers to a volume element with the dimensions x, y, and sheet thickness.

At the same time, the rate of heat flow in the area, A_{xy}, represented by a camera pixel, is dependent on the local heat transfer coefficient, h_{xy}, such as:

$$\dot{Q}_{xy}(t) = h_{xy} \cdot A_{xy} \cdot \left(T_{\text{metal},xy}(t) - T_{\text{water}}\right). \tag{3}$$

Consequently, possible changes in the heat transfer coefficient lead to changes in temperature reduction. Nevertheless, it must be considered that not the temperatures on the wetted side are measured, but the temperatures on the dry rear side of the metal sheet. This results in delayed temperature information and less detailed information due to the transverse heat conduction occurring inside the sheet.

The temperature reduction can be determined separately for the three different operating modes of the spraying tool. Thus, the detection of the cooing performance enables an independent examination of the water-bearing system and the air-bearing system. For the following test series, injections under different operating modes—straight water injection, sole air injection, and spray injection—are repeated ten times each. For a simple and meaningful evaluation, the cooling is considered exclusively at the point of maximum temperature reduction of each wetting area, while it was found in pre-investigations that the tendencies of the average temperatures within the wetted areas follow the tendencies of the maximum temperature reductions.

3.5.1. Cooling of straight water injection. In the first step, the temperature curve during the injection of pure water is investigated. An initial assumption was that the nozzles with large holes might cool the sheet metal more strongly and thus cause more pronounced temperature reductions. However, when determining the cooling of the sheet metal, it turns out that the cooling effect of large and small nozzles is approximately the same. This can be verified by the cooling pattern shown in figure 9. There are only small deviations between the individual nozzles. Due to the strong and focused impact of the water, the heat transfer coefficient reaches a high value. Obviously, the occurring variation of the heat transfer coefficient between the spray jets is relatively small compared to the absolute magnitude of the heat transfer coefficients. However, this is a special case for straight water injection.

To visualize the process of cooling and to allow comparisons, figure 13 shows the mean temperature curve derived from averaging all nine nozzles. The curve shows that the injection causes a steep drop in temperatures of about 17 K.

From the low sensitivity of cooling to nozzle hole size, it can be concluded, that problems in the water-bearing system may not be detected by evaluating the temperature reduction. However, if a change in the recorded temperature reduction of a nozzle would occur it will be a hint of an unwanted defect in the water-bearing system of the spraying tool.

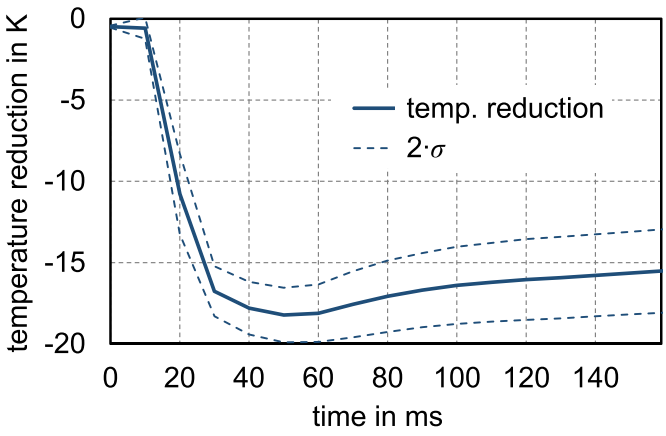

Figure 13. Mean temperature reduction over time resulting from straight water injection as an average value of all nine nozzles and ten repetitions.

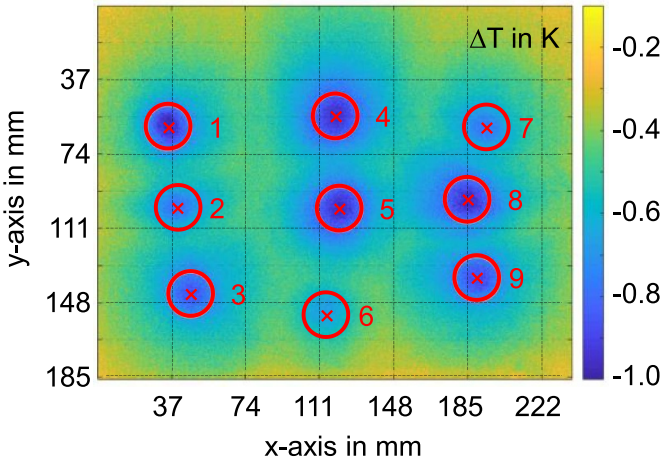

Figure 14. Cooling pattern resulting from sole air injection with markings at the individual positions of the cooling centers.

3.5.2. Cooling of a sole air injection. To determine the cooling effect of the atomizing air, the air is blown onto the heated metal sheet. It must be taken into account, that the air—in contrast to the water jet—emerges from the six outer nozzle holes, shown in figure 4. An example of the cooling pattern, resulting from sole air injection is given in figure 14. It looks similar to the cooling pattern of the spray injection, but the absolute temperature reductions are much smaller.

It can be seen that the large nozzles (number 1, 3, 4, 5, 8, and 9) induce a stronger cooling than the smaller nozzles. Therefore, figure 15 displays the average temperature decrease with the corresponding standard deviations for large and small nozzle holes, separately.

The diagram shows, that after a period of 160 ms the large nozzles produce cooling of up to 0.8 K, while the small nozzles only reach 0.4 K. The temperature reduction with air injection is much smaller than with water injection. This is due to the lower heat transfer coefficient.

Based on the differences between the nozzles with small holes and the nozzles with large holes, it can be concluded that

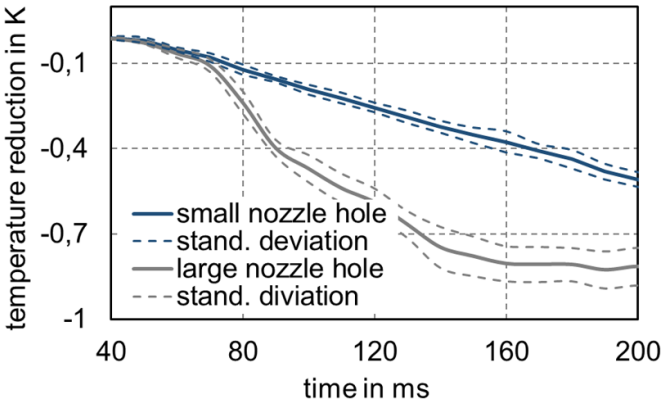

Figure 15. Mean temperature reduction over time resulting from sole air injection as average value separately for nozzles with large holes and nozzles with small holes.

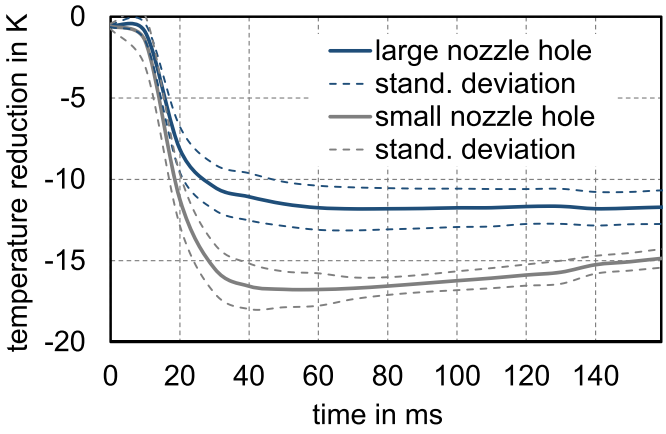

Figure 16. Mean temperature reductions over time resulting from spray injection as average value separately for nozzles with large holes and nozzles with small holes.

problems like clogging can be detected via the measurement of cooling.

For a meaningful comparison of states in the course of the life cycle, a fixed time step must be defined to determine changes in cooling. Under the present conditions, a time of 160 ms can be recommended.

3.5.3. Cooling of spray injection. Figure 10 shows the cooling pattern, which results from a spray injection, with water and atomizing air turned on. Interestingly, the small nozzles induce a stronger cooling than the nozzles with large holes. Compared to the nozzles with small holes, more air escapes from the nozzles with large holes, which causes the spray plume to have a larger radial extension. The spray plume widens further and the water droplets are distributed on the metal sheet over a larger area. This leads not only to a larger wetting surface (see figure 12) but also to reduced local cooling.

The measured maximum temperature reductions of the individual wetting surfaces are very reproducible. The standard deviation of the temperature reduction can be determined for each individual nozzle from repeated tests. If the two standard deviations of all nozzles are taken and averaged over all nozzles, a value of 0.73 K is obtained. Thus, in the case of a later single injection, it can be assumed that the deviation from the true value is very small or the deviation is presumed to be smaller than 0.73 K. Accordingly, temperature reductions are suitable as evaluation parameters. If more precise statements on the changes in temperature reduction are required in a later test, this can be achieved by carrying out repetitive measurements.

The curves plotted in figure 16 show the temperature reductions in the centers of the wetted areas over time, which in turn result from the average values of the various nozzles. During the injection of the nozzles with large holes, the sheet temperature drops by 12 K, while nozzles with small holes cause an increased cooling of 17 K. This illustrates the great importance of the atomization process for wetting and cooling.

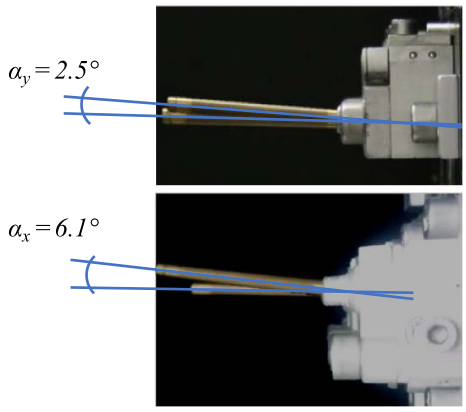

Figure 17. Side view (upper image) and top view (lower image) of nozzle 8. To measure the shift of the orientation, a pin was locked to the nozzle. The angle is plotted in the superimposed images.

Overall it can be concluded, that the evaluation of the cooling allows detecting obstructions of the air outlet holes or the entire air-bearing system. In turn, it is not possible to find small changes in the flow rate within the water-bearing system. For a simplified but meaningful comparison of different measurements, a fixed point in time must be selected for the comparison.

3.6. Test case for nozzle alignment

In an additional step, a proof of concept was carried out with the help of a defined test case. For this purpose, the orientation of nozzle 8 was changed (see the position in figure 14). To record the change in direction as precisely as possible, a small pin was fixed in the nozzle mouth. The alignment of the nozzle can be determined with the aid of photos taken from above and from the side. In figure 17, the photos are superimposed before and after the change in direction and the angles are plotted. With the angle and the known distance of 11 cm between nozzle and metal plate, the theoretically expected displacement of the wetted surface can be determined.

Table 4. Shift of the center of the wetted area of nozzle 8 before and after the nozzle adjustment during the injection of water and spray, left: theoretical values from the side view images, right: measured values from the wetted areas.

	α_x	α_y	Δx-pos (mm)	Δy-pos (mm)	Δx-pos (mm)	Δy-pos (mm)
Operating mode	Theoretical values				Measurement	
Pure water	6.1°	2.5°	−11.8	−4.8	−13.5	−4.6
Spray					−12.2	−3.9

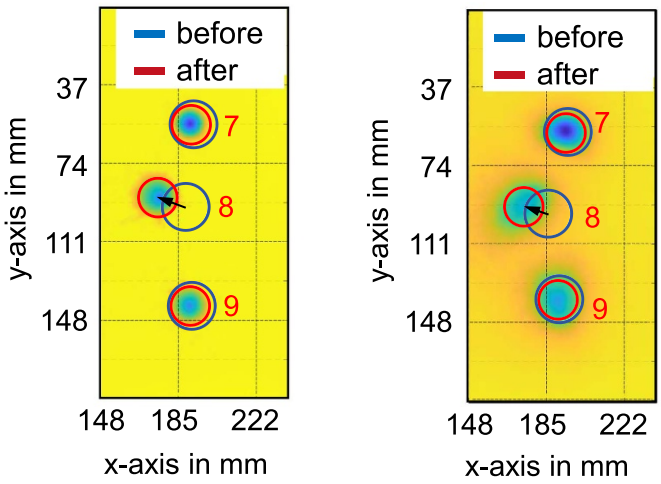

Figure 18. IR-images with points of impact before (blue) and after (red) the realignment of nozzle 8, left: straight water injection, right: spray injection.

The results are documented in table 4 with the angles in x and y-position and the expected theoretical displacement of 11.8 mm in x-direction and 4.8 mm in y-direction.

This evaluation is followed by the wetting experiments. The images of the IR-wetting patterns are shown in figure 18, on the left for the injection of pure water and on the right for the spray injection. The experiments have been performed with all nine nozzles. For ease of comparison, only the third nozzle column has been mapped. The circles added have their center in the calculated center of the wetted area, blue for the positions before adjustment and red for the positions after adjustment. Each position shown is based on only a single injection. It can be seen that nozzle 8—which has been adjusted—deviates significantly from the previous positions of the jet impact, whereas the remaining nozzles are close to the original position.

Finally, the shift of the center positions of the wetted areas of nozzle 8 before and after adjustment are determined and documented in table 4 in the 'measurement' column. In the cases of straight water injection and spray injection, there are small differences in the determined position shift. The difference is 1.3 mm in the x-direction and 0.7 mm in the y-direction. Since the tests are single measurements, the deviation can be attributed to the occurring variance. A deviation of the center position of 1.3 mm can also be considered minor.

Table 5. Summary of the control recordings and recommended belonging evaluation parameters.

Recordings	Evaluation parameter
Air injection	Temperature reduction.
Straight water injection	Position of wetted area, size of wetted area.
Spray injection	Position of wetted area, size of wetted area, temperature reduction.

If the wetting results are compared with the previously obtained theoretical shifts, a slight deviation can be observed as well. This can have various causes. In particular, the limited accuracy of the angle measurements. In summary, it can be stated that a change in nozzle orientation can be detected. The determined absolute values are subject to various influences, which leads to small deviations between the expected and actual measured values.

3.7. Fault detection on nozzle arrays

The method presented enables quick and reliable identification of individual faulty nozzles in a large array of nozzles. In addition, the method allows further narrowing down of problems that have occurred. This can be followed by a targeted correction or repair. It must be explicitly pointed out that the operation of spraying tools, as well as spray formation and spray propagation, involve very complex processes. Small changes in the boundary conditions can cause different changes in the measured wetting patterns. Therefore, it is never possible to identify errors with absolute certainty and the fault assignment presented here should not be seen as an exclusive possibility. In order to get a better overview between possible errors and the different operating conditions and setting parameters, a summary now follows.

The prerequisite for carrying out an evaluation is the recording of master images and control images. Since there are three operating modes, the master images and the control images must be recorded for each of these operating modes. The operating modes are: sole air injection, straight water injection, and spray injection.

There are three possible evaluation parameters: position of the wetted area, size of the wetted area, and temperature reduction. From the recordings of the straight water injection and spray injection, the position of the wetted area and the size of the wetted area need to be determined for each nozzle. From the recordings of the spray injection and the sole air injection, the temperature reduction can be evaluated additionally. In table 5, the recommended evaluation parameters are assigned to the recordings of the operating modes.

Unwanted changes or defects can be detected by comparing the results between the master image and the control images. Table 6 contains a list of possible defects. The individual defects have been assigned to certain measurement results by which the corresponding defect can be inferred. For example, a decreased size of wetted area during straight water injection of a nozzle is likely to be caused by a decreased water mass

Table 6. Correlation between occurring measurement results and the possible causes in the spraying tool.

Measurement result	Possible malfunction
Shift of the position of the center point of the wetted area	
During straight water injection and spray injection	Changed jet orientation due to misalignment of corresponding nozzle.
Only during straight water injection	Problems in the water-bearing system of corresponding nozzle.
Only during spray injection	Problems in the air-bearing system of corresponding nozzle.
Decrease of the size of wetted area	
During straight water injection	Water mass flux decreased; decreased water pressure or clogging of the water-bearing system of corresponding nozzle, faulty control valve (see figure 3).
During spray injection	Air mass flux decreased; decreased air pressure or clogging of the air-bearing system of corresponding nozzle, faulty control valve (see figure 3).
Decreased temperature reduction	
During air injection	Decreased air volume flux.
or during spray injection	Decreased air pressure or clogging of the air-bearing system of corresponding nozzle.

flux which can result from decreased water pressure or clogging of the water-bearing system of the corresponding nozzle.

In the table, only the main conclusions are listed, but of course, many related changes can occur, which then allow further narrowing down of the problems. An important distinction must be made regarding whether changes occur only at individual nozzles or whether changes occur at all nozzles. If changes occur for all nozzles at the same time, then problems in the central water or air supply are very likely.

The described method can also be used for other types of spraying tools and nozzles. However, if nozzles are used that have only one operating mode, such as simple pressure-jet atomizers, then the measurement results are less comprehensive, compared to nozzles with three operating modes. For this reason, it can then be more difficult to assign possible malfunctions. It is important to note that the basic measuring principle, the detection of changes compared to a target state, remains the same. Thus, changes in the qualitative wetting pattern and quantitative changes in the wetting pattern (positions of center points, sizes of the wetted areas, or maximum cooling) can be identified. From these data, various possible malfunctions can be narrowed down analogously to table 6, for all kinds of spraying tools.

4. Conclusions

Complex multi-nozzle spraying tools pose challenges for conventional measuring systems. Especially when an application under harsh industrial conditions is required. In many industrial applications, continuous documentation of the spray quality is required to guarantee product quality and ensure uninterrupted production. The absolute values of parameters such as droplet diameter and velocity or spray cone diameter are usually not of particular interest, but rather whether the spraying tool produces a consistent wetting of the mold or casting.

For this purpose, we have developed and tested a method that allows continuous monitoring of complex sprays. The method is based on the wetting pattern generated by the spray on the surface of a heated metal plate. This pattern is captured on the back of the plate by an infrared camera. The monitoring is built on master recordings taken with a properly functioning spraying tool. Subsequent regular recordings of control images allow comparison with the master image. Changes between master and control images indicate changes in the spray tool.

To characterize the performance of the new method in more detail, a spraying tool with nine external mixing air–water nozzles was used. With the new infrared method, the three working modes (air injection, straight water injection, spray injection) of a spraying tool can be investigated separately. The investigations have shown that the evaluation parameters (position of wetted area, size of wetted area, temperature reduction) can be recorded with high sensitivity and precision. For example, the position of the wetted area of a nozzle can be determined with a precision of 0.42 mm. This allows even the smallest changes in nozzle orientation to be detected. Based on the evaluation parameters, possible defects can be deduced, these include:

- detection of faulty nozzles
- the directional adjustment of an individual nozzle or multiple nozzles
- the partial or complete blockage of the water access of individual or multiple nozzles
- the partial or complete blockage of the air access of individual or multiple nozzles
- faulty control valves of an individual nozzle or multiple nozzles
- problems in the central water supply
- problems in the central air supply.

The rapid and reliable identification of problems prevents the production of rejects and long production downtimes. At the same time, the method helps to optimally design spraying tools and adapt them to new mold geometries. Thus, the

presented new infrared pattern method enables fast, robust, and cost-effective monitoring of complex spray tools.

Data availability statement

The data that support the findings of this study are available upon reasonable request from the authors.

ORCID iDs

Florian Schulz https://orcid.org/0000-0002-7818-2823
Frank Beyrau https://orcid.org/0000-0002-8043-7194

References

Dafsari R A, Vashahi F, Chandrahasan R and Lee J 2019 Effect of aviation fuel temperature on refractive index in droplet size measurement using phase Doppler anemometry *Meas. Sci. Technol.* **30** 75203

Emberson D R, Ihracska B, Imran S and Diez A 2016 Optical characterization of diesel and water emulsion fuel injection sprays using shadowgraphy *Fuel* **172** 253–62

Fansler T D and Parrish S E 2015 Spray measurement technology: a review *Meas. Sci. Technol.* **26** 12002

Hult J and Mayer S 2013 A methodology for laser diagnostics in large-bore marine two-stroke diesel engines *Meas. Sci. Technol.* **24** 45204

Kim D, Park S S and Bae C 2018 Schlieren, shadowgraph, Mie-scattering visualization of diesel and gasoline sprays in high pressure/high temperature chamber under GDCI engine low load condition *Int. J. Automot. Technol.* **19** 1–8

Mantel R 2017 Über die Interaktion fast paralleler sowie kollidierender Kraftstoffsprays *Scientific Research Dissertation* Universitäts- und Landesbibliothek Darmstadt, Darmstadt

Montanaro A, Allocca L, Meccariello G and Lazzaro M 2015 Schlieren and Mie scattering imaging system to evaluate liquid and vapor contours of a gasoline spray impacting on a heated wall *12th Int. Conf. on Engines & Vehicles* (*SAE Technical Paper Series)* (*Warrendale, PA, United States*, *13 September 2015*)

Nocivelli L, Montenegro G, Onorati A, Curto F, Eggenschwiler PD, Liao Y, Vogel A 2017 Quantitative analysis of low pressure-driven spray mass distribution and liquid entrainment for SCR application through a mechanical patternator *WCX™ 17: SAE World Congress Experience (SAE Technical Paper Series)* (*Warrendale, PA, United States*, *4 April 2017*)

Parrish S E and Zink R J 2013 Development and application of a high-speed planar laser-induced fluorescence imaging system to evaluate liquid and vapor phases of sprays from a multi-hole diesel fuel injector *Meas. Sci. Technol.* **24** 25402

Rahim E A and Dorairaju H 2018 Evaluation of mist flow characteristic and performance in minimum quantity lubrication (MQL) machining *Measurement* **123** 213–25

Schulz F and Beyrau F 2017 The influence of flash-boiling on spray-targeting and fuel film formation *Fuel* **208** 587–94

Schulz F, Reincke F, Mrochen M and Beyrau F 2021 A measuring system for monitoring multi-nozzle spraying tools *Meas. Sci. Technol.* **32** 055902

Schulz F, Samenfink W, Schmidt J and Beyrau F 2016 Systematic LIF fuel wall film investigation *Fuel* **172** 284–92

Schulz F, Schmidt J, Kufferath A and Samenfink W 2014 Gasoline wall films and spray/wall interaction analyzed by infrared thermography *SAE Int. J. Engines* **7** 1165–77

Serras-Pereira J, Aleiferis P G and Richardson D 2015 An experimental database on the effects of single- and split injection strategies on spray formation and spark discharge in an optical direct-injection spark-ignition engine fuelled with gasoline, iso-octane and alcohols *Int. J. Engine Res.* **16** 851–96

Wigley G, Hargrave G K and Heath J 1999 A high power, high resolution LDA/PDA system applied to gasoline direct injection sprays *Part. Part. Syst. Charact.* **16** 11–19

Zhang M, Min X, Zhang Y, Zhang G and Cleary D J 2012 Flow-field investigation of multi-hole superheated sprays using high-speed PIV. Part I. Cross-sectional direction *At. Sprays* **22** 983–95